GNSS Avionics-Based Integrity Augmentation for RPAS Detect-and-Avoid Applications

Roberto Sabatini
School of Aerospace, Mechanical and Manufacturing Engineering
RMIT University, Melbourne, VIC 3000, Australia
roberto.sabatini@rmit.edu.au

Terry Moore and Chris Hill
Nottingham Geospatial Institute
University of Nottingham, NG7 2TU, UK

Abstract: Taking the move from our recent research on GNSS Avionics Based Integrity Augmentation (ABIA), this article investigates the synergies of ABIA with a novel Detect-and-Avoid (DAA) architecture for Remotely Piloted Aircraft System (RPAS). Based on simulation and experimental data collected on a variety of manned and unmanned aircraft, it was observed that the integration of ABIA with DAA has the potential to provide an integrity-augmented DAA for both cooperative and non-cooperative applications. The candidate DAA system uses various Forward-Looking Sensors (FLS) for the non-cooperative case and Automatic Dependent Surveillance-Broadcast (ADS-B) in addition to TCAS/ASAS for the cooperative case. Both in the cooperative and non-cooperative cases, the risk of collision is evaluated by setting a threshold on the Probability Density Function (PDF) of a Near Mid-Air Collision (NMAC) event over the separation area. So, if the specified threshold is exceeded, an avoidance manoeuvre is performed based on a heading-based Differential Geometry (DG) algorithm and optimized utilizing a cost function with minimum time constraints and fuel penalty criteria weighted as a function of separation distance. Additionally, the optimised avoidance trajectory considers the constraints imposed by the ABIA in terms of RPAS platform dynamics and GNSS constellation satellite elevation angles, preventing degradation or losses of navigation data during the whole DAA loop. This integration scheme allows real-time trajectory corrections to re-establish the Required Navigation Performance (RNP) when actual GNSS accuracy degradations and/or data losses take place (e.g., due to aircraft-satellite relative geometry, GNSS receiver tracking, interference, jamming or other external factors). Cooperative and non-cooperative simulation case studies were accomplished to evaluate the performance of this Integrity-Augmented DAA (IAS) architecture. The selected host platform was the AEROSONDE RPAS and the simulation cases were performed in a representative cross-section of the RPAS operational flight envelope. The simulation results show that the proposed IAS architecture is capable of performing high-integrity conflict detection and resolution when GNSS is the primary source of navigation data.

Introduction

In addition to Space Based Augmentation Systems (SBAS) and Ground Based Augmentation Systems (GBAS), Global Navigation Satellite System (GNSS) augmentation can also take the form of additional information being provided by other avionic systems. In most cases, the additional avionic systems operate via separate principles than the GNSS and, therefore, are not subject to the same sources of error or interference. A system such as this is referred to as an Avionics-Based or Aircraft-Based Augmentation System (ABAS). While GBAS and SBAS address all four cornerstones of GNSS performance augmentation (i.e., accuracy, integrity, availability and continuity), the ABAS approach is particularly well suited to increase the levels of integrity and accuracy of GNSS in a variety of mission- and safety-critical aviation applications. In RPAS applications, airworthiness drivers for both cooperative and non-cooperative Detect-and-Avoid (DAA) impose stringent GNSS data integrity requirements. Therefore, a properly designed and certifiable Avionics Based Integrity Augmentation (ABIA) capability would allow an extended spectrum of autonomous and safety-critical operations by continuously monitoring GNSS integrity levels and providing suitable caution and warning signals to the remote pilot or to the avionics flight control systems in order to accomplish GNSS-based mission and safety-critical tasks. This increased level of integrity could provide a pathway to support the challenging task of RPAS certification for unrestricted access to commercial airspace. Although current and likely future SBAS/GBAS augmentation systems can provide significant improvement of GNSS navigation performance, a properly designed and flight certified ABAS/ABIA system could play a key role in GNSS integrity augmentation for aviation safety-critical applications, including RPAS DAA. Furthermore, using suitable data link and data processing technologies on the ground, a certified ABAS/ABIA capability could be one of the core elements of a future GNSS Space-Ground-Avionics Augmentation Network (SGAAN).

ABIA Research

Previous research on ABIA systems demonstrated the potential of this technology to enhance GNSS integrity performance in a variety of mission- and safety-critical applications including experimental

flight test/flight inspection, precision approach and automatic landing [1-5]. Therefore, an advanced ABIA system was developed for RPAS applications (Figure 1). In this system, the on-board sensors provide information on the aircraft relevant flight parameters (navigation data, engine settings, etc.) to an Integrity Flag Generator (IFG), which is also connected to the GNSS system. Using the available data on GNSS and the relevant aircraft flight parameters, integrity signals are generated which can be sent to the RPAS Ground Station (RGS) or used by a Flight Path Optimisation Module (FPOM). This system addresses both the predictive and reactive nature of GNSS integrity augmentation by producing suitable integrity flags (cautions and warnings) in case of predicted/ascertained GNSS data losses or unacceptable signal degradations exceeding the Required Navigation Performance (RNP) specified for each phase of flight, and providing guidance information to the remote pilot/autopilot to avoid further data losses/degradations.

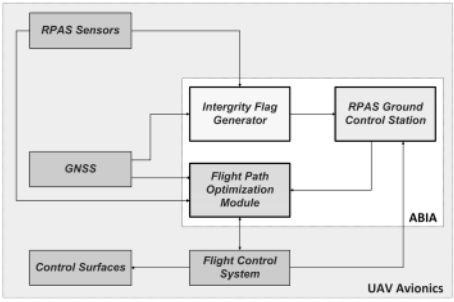

Figure 1 ABIA system architecture for RPAS applications

To achieve this, an Integrity Flag Generator (IFG) module produces the following integrity flags [1-3]:

- **Caution Integrity Flag (CIF):** a predictive annunciation that the GNSS data delivered to the avionics system is going to exceed the RNP thresholds specified for the current and planned flight operational tasks (GNSS alert status).
- **Warning Integrity Flag (WIF):** a reactive annunciation that the GNSS data delivered to the avionics system has exceeded the RNP thresholds specified for the current flight operational task (GNSS fault status).

The following definitions of Time-to-Alert (TTA) are applicable to the ABIA system [1]:

- **ABIA Time-to-Caution (TTC):** the minimum time allowed for the caution flag to be provided to the user before the onset of a GNSS fault resulting in an unsafe condition.
- **ABIA Time-to-Warning (TTW):** the maximum time allowed from the moment a GNSS fault resulting in an unsafe condition is detected to the moment that the ABIA system provides a warning flag to the user.

ABIA Integrity Flag Generator (IFG)

The main causes of GNSS data degradation or signal losses in aviation applications were deeply analysed in [1] and are listed below:

- Antenna obscuration (i.e., obstructions from the wings, fuselage and empennage during maneuvers);
- Adverse satellite geometry, resulting in high Position Dilution of Precision (PDOP);
- Fading, resulting in reduced carrier-to-noise ratios (C/N_0);
- Doppler shift, impacting signal tracking and acquisition/reacquisition time;
- Multipath effects, leading to a reduced C/N_0 and to range/phase errors;
- Interference and jamming.

Understanding the physics of these phenomena and developing reliable mathematical models was essential in order to properly design the ABIA IFG module [1, 2]. Figure 2 shows the architecture of the IFG module and its interfaces.

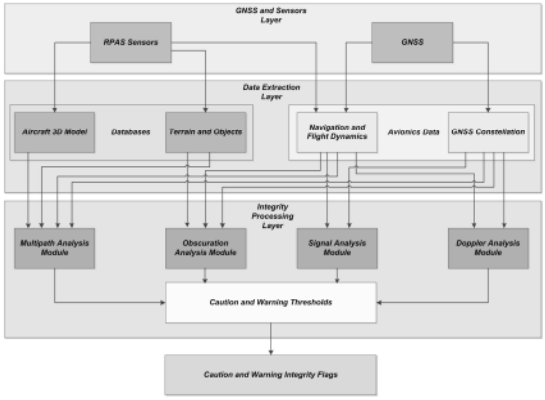

Figure 2 ABIA IFG module architecture

The ABIA IFG module is designed to provide CIF and WIF alerts in real-time (i.e., in accordance with the specified TTC and TTW requirements in all relevant flight phases). IFG module inputs are from the GNSS receiver and other aircraft sensors. The GNSS and Sensors Layer (GSL) passes the aircraft Position, Velocity, Time (PVT) and attitude (Euler angles) data (from the on board Inertial Navigation Systems, Air Data Computer, etc.), GNSS data (raw measurements and PVT) and the Flight Control System (FCS) actuators data to the Data Extraction Layer (DEL). At this stage, the required Navigation and Flight Dynamics (NFD) and GNSS Constellation Data (GCD) are extracted, together with the relevant information from an aircraft Three-Dimensional Model (3DM) and from a Terrain and Objects Database (TOD). The 3DM database is a detailed

geometric model of the aircraft built in a Computer Aided Three-dimensional Interactive Application (CATIA). The TOD uses a Digital Terrain Elevation Database (DTED) and additional man-made objects data to obtain a detailed map of the surfaces neighbouring the aircraft. In the Integrity Processing Layer (IPL), the Doppler Analysis Module (DAM) calculates the Doppler shift by processing the NFD and GCD inputs. The Multipath Analysis Module (MAM) processes the 3DM, TOD, GNSS Constellation Module (GCM) and A/C Navigation/Dynamics Module (ADM) inputs to determine multipath contributions from the aircraft (wings/fuselage) and from the terrain/objects close to the aircraft. The Obscuration Analysis Module (OAM) receives inputs from the 3DM, GCS and ADS, and computes the GNSS antenna obscuration matrixes corresponding to the various aircraft manoeuvres. The Signal Analysis Module (SAM) calculates the C/N_0 of the direct GNSS signals received by the aircraft in the presence of atmospheric propagation disturbances, as well as the applicable radio frequency interference and Jamming-to-Signal ratio (J/S) levels. The Integrity Flags Layer (IFL) uses a set of predefined CIF/WIF threshold parameters to trigger the generation of both caution and warning flags associated with antenna obscuration, Doppler shift, multipath, carrier, interference and satellite geometry degradations. The approach adopted to set-up thresholds for the ABIA CIF and WIF integrity flags is depicted in Figure 3. The masking integrity flag criteria are the following:

- When the current aircraft manoeuvre will lead to less than 4 satellite in view, the CIF shall be generated.
- When less than 4 satellites are in view, the WIF shall be generated.

Additionally, when only four satellites are in view:

- When one (or more) satellite(s) elevation angle (antenna frame) is less than 10 degrees, CIF shall be generated.
- When one (or more) satellite(s) elevation angle is less than 5 degrees, WIF shall be generated.

From the definition of Dilution of Precision (DOP) factors, GNSS accuracy can be expressed by [6]:

$$\sigma_P = \mathrm{DOP} \times \sigma_{\mathrm{UERE}} \quad (1)$$

where $\sigma_P$is the standard deviation of the positioning accuracy and $\sigma_{\mathrm{UERE}}$is the standard deviation of the satellite pseudorange measurement error. Therefore, the 1-sigma Estimated Position, Horizontal and Vertical Errors of a GNSS receiver can be calculated using the PDOP (EPE in 3D), the HDOP (EHE in 2D) or the VDOP (EVE). In order to generate CIFs and WIFs that are consistent with current GNSS RNP, we need to introduce the Horizontal and Vertical Accuracy (HA/VA) requirements in the various flight phases. The Horizontal Alert Limit (HAL) is the radius of a circle in the horizontal plane, with its centre being at the true position, which describes the region which is required to contain the indicated horizontal position with the required probability for a particular navigation mode. Similarly, the Vertical Alert Limit (VAL) is half the length of a segment on the vertical axis, with its centre being at the true position, which describes the region which is required to contain the indicated vertical position with the required probability for a particular navigation mode. As a result of our discussion, the DOP integrity flags criteria are the following:

- When the EHE exceeds the HA 95% or the VA 95% alert requirements, the CIF shall be generated.
- When the EHE exceeds the HAL or the EVE exceeds the VAL, the WIF shall be generated.

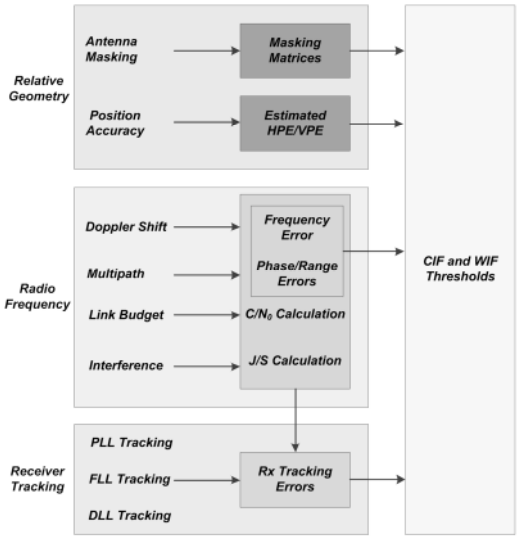

Figure 3 Integrity flag thresholds

During the landing phase, a GNSS Landing System (GLS) has to be augmented by GBAS in order to achieve the RNP, as well as Lateral and Vertical Protection Levels (LPL and VPL). LPL/VPL is defined as the statistical error value that bounds the Lateral/Vertical Navigation System Error (NSE) with a specified level of confidence. In particular, for the case of Local Area Augmentation System (LAAS), which allows for multiple Differential Global Positioning System (DGPS) reference receivers (up to four) to be implemented, two different hypotheses are made regarding the presence of errors in the measurements. These hypotheses are:

H_0 Hypothesis – No faults are present in the range measurements (includes both the signal and the receiver measurements) used in the ground station to compute the differential corrections;

H_1 Hypothesis – A fault is present in one or more range measurements and is caused by one of the reference receivers used in the ground station.

Consequently, LPL and VPL are computed as follows:

$$\mathrm{LPL} = \mathrm{MAX}\{\mathrm{LPL}_{H0}, \mathrm{LPL}_{H1}\} \quad (2)$$

$$\mathrm{VPL} = \mathrm{MAX}\{\mathrm{VPL}_{H0}, \mathrm{VPL}_{H1}\} \quad (3)$$

VPL and LPL for the H_0 and H_1 hypotheses are calculated as described in [16]. The lateral and vertical accuracy (NSE 95%) and alert limits required by a GLS in the presence of LAAS, considering the continuously varying position of the aircraft with respect to the Landing Threshold Point (LTP) are given in [7]. Additionally, [7] provides the so-called Continuity of Protection Levels in terms of Predicted Lateral and Vertical Protection Levels (PLPL and PVPL). Although the definition in [7] is quite comprehensive, a generic statement is made that the PVPL and PLPL computations shall be based on the ranging sources expected to be available for the duration of the approach. In other terms, it is implied that the airborne subsystem shall determine which ranging sources are expected to be available, including the ground subsystem's declaration of satellite differential correction availability (satellite setting information). Unfortunately, this generic definition does not address the various conditions for satellite signal losses associated to specific aircraft manoeuvres (including curved GLS precision approaches). Therefore, it is suggested that an extended definition of PLPL and PVPL is developed taking into account the continuously varying aircraft-satellite relative geometry (masking envelope). In particular, when the current aircraft manoeuvre will lead to less than 4 satellites in view or unacceptable accuracy degradations, the CIF shall be generated. Following our discussion, the additional integrity flags criteria adopted for GLS in the presence of LAAS are the following:

- When the PLPL exceeds LAL or PVPL exceeds the VAL, the CIF shall be generated.
- When the LPL exceeds the LAL or the VPL exceeds the VAL, the WIF shall be generated.

Multipath integrity flags were defined using the Early-Late Phase (ELP) observable and the range error [8]. As described in [2], the multipath integrity flags criteria are the following:

- When the ELP exceeds 0.1 radians, the caution integrity flag shall be generated.
- When the multipath range error exceeds 1 meter, the warning integrity flag shall be generated.

In order to define the integrity thresholds associated with Doppler and fading effects, a dedicated analysis of the GNSS receiver tracking performance was required. When the GNSS measurement errors exceed certain thresholds, the receiver loses lock to the satellites. Since both the code and carrier tracking loops are nonlinear, especially near the threshold regions, only Monte Carlo simulations of the GNSS receiver in different dynamics and SNR conditions can determine the receiver tracking performance [6, 9, 10]. Nevertheless, some conservative rule of thumbs that approximate the measurement errors of the GNSS tracking loops can be used. Numerous sources of measurement errors affect the Phase Lock Loop (PLL) and the Frequency Lock Loop (FLL). However, for our purposes, it is sufficient to analyze the dominant error sources in each type of tracking loop. Considering a typical GNSS receivers employing a two-quadrant arctangent discriminator, the PLL threshold is given by [6]:

$$3\sigma_{\mathrm{PLL}} = 3\sigma_j + \theta_e \leq 45^{\circ} \quad (4)$$

where:

σ_j = 1-sigma phase jitter from all sources except dynamic stress error;

θ_e = dynamic stress error in the PLL tracking loop.

Frequency jitter due to thermal noise and dynamic stress error are the main errors in a GNSS receiver FLL. The receiver tracking threshold is such that the 3-sigma jitter must not exceed one-fourth of the frequency pull-in range of the FLL discriminator. Therefore, the FLL tracking threshold is [6]:

$$3\sigma_{\mathrm{FLL}} = 3\sigma_{\mathrm{tFLL}} + f_e \leq 1/4T \ \ (\mathrm{Hz}) \quad (5)$$

where:

$3\sigma_{\mathrm{FLL}}$ = 3-sigma thermal noise frequency jitter;

σ_{tFLL}= dynamic stress error in the FLL tracking loop.

Regarding the code tracking loop, a conservative rule-of-thumb for the Delay Lock Loop (DLL) tracking threshold is that the 3-sigma value of the jitter due to all sources of loop stress must not exceed the correlator spacing (d), expressed in chips. Therefore [6]:

$$3\sigma_{\mathrm{DLL}} = 3\sigma_{\mathrm{tDLL}} + R_e \leq d \ \ (\mathrm{chips}) \quad (6)$$

where:

σ_{tDLL} = 1-sigma thermal noise code tracking jitter;

R_e = dynamic stress error in the DLL.

The Phase Lock Loop (PLL), FLL and DLL error models described in [2] allow determining the C/N_0 corresponding to the receiver tracking thresholds. The Scalar Tracking Loops (STL) typically employ Delay Lock Loops (DLL) to track the code phase and Phase Lock Loops (PLL) or Frequency Lock Loops (FLL) to track the carrier phase. State-of-the-art STL also employ combined PLL and FLL for carrier tracking to obtain better results in navigation position accuracy and enhanced tracking. Recently, Vector

Tracking Loops (VTL) have been employed, which are based on an advanced receiver architecture capable of tracking signals in a combined manner. VTL has the advantage of operating at a lower total carrier power to noise ratio (C/No) and in higher manoeuvrability when compared to STL logics. The general C/N_0 integrity flag criterion applicable to the ABIA system is:

$$\left(\frac{C}{N_0}\right)_{\text{Threshold}} = \max\begin{bmatrix} \left(\frac{C}{N_0}\right)_{\text{PLL}}, \\ \left(\frac{C}{N_0}\right)_{\text{FLL}}, \left(\frac{C}{N_0}\right)_{\text{DLL}}, \\ \left(\frac{C}{N_0}\right)_{\text{PLL+FLL}}, \left(\frac{C}{N_0}\right)_{\text{VTL}} \end{bmatrix} \quad (7)$$

where $(C/N_0)_{\text{PLL}}$ is the minimum C/N_0 for PLL tracking, $(C/N_0)_{\text{FLL}}$ is the minimum C/N_0 for FLL tracking, $(C/N_0)_{\text{DLL}}$ is the minimum C/N_0 for DLL tracking, $(C/N_0)_{\text{PLL+FLL}}$ is the minimum C/N_0 for combined PLL and FLL tracking and $(C/N_0)_{\text{VTL}}$ is the minimum C/N_0 for VTL based tracking. Numerical solutions of Eqs. (4), (5) and (6) show that the weak link in unaided avionics GNSS receivers is the carrier tracking loop threshold (greater sensitivity to dynamics stress). Therefore, the $(C/N_0)_{\text{PLL}}$ threshold can be adopted in these cases. In general, when the PLL loop order is made higher, there is an improvement in dynamic stress performance. Therefore, third order PLL are widely adopted in avionics GNSS receivers. Assuming 15 to 18 Hz noise bandwidth and 5 to 20 msec predetection integration time (typical values for avionics receivers), the rule-of-thumb tracking threshold for the PLL gives 25 to 28 dB-Hz. Additionally, in aided avionics receiver applications, the PLL tracking threshold can be significantly reduced by using external velocity aiding in the carrier tracking loop. With this provision, a tracking threshold of approximately 15 to 18 dB-Hz can be achieved. Using these theoretical and experimental threshold values, we can also calculate the receiver Jamming-to-Signal (J/S) performance for the various cases of practical interest, as described in [1]. When available, flight test data collected in representative portions of the aircraft operational flight envelope (or the results of Monte Carlo simulation) shall be used. Taking an additional 5% margin on the 3-sigma tracking thresholds for the CIF, the following additional criteria are introduced for the ABIA integrity thresholds:

- When either $42.25° \leq 3\sigma_{\text{PLL}} \leq 45^{\circ}$ or $0.2375\text{T} \leq 3\sigma_{\text{FLL}} \leq 0.25\text{T}$ or $0.05\text{d} \leq 3\sigma_{\text{DLL}} \leq \text{d}$, the CIF shall be generated.
- When either $3\sigma_{\text{PLL}} > 45^{\circ}$ or $3\sigma_{\text{FLL}} > 1/4T$ or $3\sigma_{\text{DLL}} > d$ the WIF shall be generated.

In avionics receivers, lock detectors are used to assess if the satellite signals are being tracked or not tracked. Code lock detection is very similar to estimating the received C/N_0, inferring that the receiver is operating on or near the correlation peak. Knowledge of code lock is obviously parallel to the knowledge of received signal power. The receiver's code-correlation process has to raise the signal out of the noise. The spread spectrum processing gain (G_p) is defined as the ratio of the spread bandwidth to the unspread (baseband) bandwidth and is expressed in dB. The post-correlation signal-to-noise ratio can be calculated by [11]:

$$(S/N)_{\text{post-corr.}} = (S/N)_{\text{pre-corr.}} + G_p \quad (8)$$

When the receiver code is aligned with the transmitted code, the signal power at the band pass output is crushed into approximately 100 Hz of bandwidth. The processing gain can be calculated from:

$$G_P = 10\log\left(\frac{2C_R}{T_D}\right) \text{ (dB)} \quad (9)$$

where C_R is the chipping rate and T_D is the data period. For the C/A-code this works out to be about 43 dB. Typical avionics receivers have a cut off value at 10 dB, which means that if the value is less than this the satellite signal level is too low to be used in the positioning computations [12]. Therefore, an additional threshold to be accounted for is:

$$S/N_{\text{post-corr.}} = S/N_{\text{pre-corr.}} + G_p \geq 10 \text{ dB} \quad (10)$$

During experimental flight test activities performed with unaided L1 C/A code avionics receivers, it was also found that, in a variety of dynamics conditions, a C/N_0 of 25 dB-Hz was sufficient to keep tracking of the satellites [11]. Consequently, taking a 2 dB margin for the CIF, the following criteria are adopted for the S/N integrity flags:

- When the C/N_0 is less than 27dB-Hz or the difference between the S/N and the processing gain is less than 12 dB, the CIF shall be generated.
- When the C/N_0 is less than 25dB-Hz or the difference between the S/N and the processing gain is less than 10 dB, the WIF shall be generated.

Additionally, with reference to the individual satellites being tracked, the following additional criteria are defined:

- The CIF is triggered if there are less than 5 satellites in view (without any individual satellite CIF)
- The WIF is triggered if less than 5 satellites are remaining with one or more individual satellite CIF.

The ABIA system monitors the GNSS performances and gathers appropriate data to detect a departure

from the nominal service state. The system also reports aberrant behaviour to the pilot/autopilot who in turn is responsible for acting to either modify the aircraft trajectory (or terminate the service). The functions are performed in a sequential manner and each function is modelled as a time-to-complete process. The cumulative sum of all four function completion times defines the time required for their associated integrity assurance process to respond to a navigation service failure. The response model provides the overall time-to-complete by considering the times required for monitoring, detecting, reporting and reacting (computing and commanding an optimised trajectory free from GNSS data degradations) and is given by [1, 14]:

$$\Delta t_{respond} = \Delta t_{monitor} + \Delta t_{detect} + \Delta t_{report} + \Delta t_{react} \quad (13)$$

ABIA Flight Path Optimisation Module

The ABIA FPOM performs the fundamental task optimising the RPAS trajectory in line with the ABIA IFG constraints (CIF/TTC and WIF/TTW). This problem can be solved like other optimal control problems by using a variety of direct or indirect methods. In the initial implementation, a standard Gauss pseudospectral transcription method was adopted. However, other techniques can be adopted for the FPOM module based on numerical performance requirements (rate of convergence, stability, etc.) for the specific flight task at hand. In particular, simpler/faster geometric optimisation algorithms can be adopted to ensure the real-time performance of the trajectory optimisation task in safety-critical DAA applications (e.g., close mid-air encounters). The ABIA FPOM architecture is depicted in Figure 4.

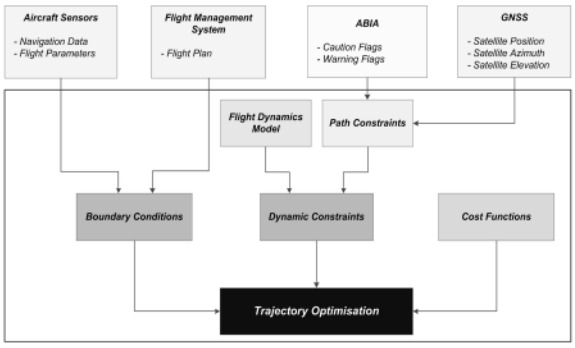

Figure 4 ABIA FPOM architecture

The RPAS flight dynamics and the IFG driven path constraints provide the full set of dynamic constraints to generate flyable trajectories. The boundary conditions include minimum, maximum, initial and final values for the state and command variables. These are provided by the aircraft sensors (i.e., current flight parameters), and by the FMS (i.e., flight plan data). The cost functions represent the performance criteria that must be minimized. As all necessary IFG constraints are already included in the path constraints, the cost functions are based on a number of key parameters, including minimum time and minimum fuel (fuel penalty) criteria.

RPAS Dynamics Model

The aircraft dynamics model is a 3-Degree of Freedom (3-DoF) point mass and unsteady flight model with variable mass (due to fuel consumption). The full set of 3-DOF scalar equations is:

$$\frac{dV}{dt} = \frac{T}{m}\cos\alpha - \frac{D}{m} - g\sin\gamma \quad (14)$$

$$\frac{d\gamma}{dt} = \left(\frac{T}{mV}\sin\alpha + \frac{L}{mV}\right)\cos\varphi - \frac{g}{V}\cos\gamma \quad (15)$$

$$\frac{d\psi}{dt} = (T\sin\alpha + L)\frac{\sin\varphi}{mV\cos\gamma} \quad (16)$$

$$\frac{dm}{dt} = -s_{sfc}T \quad (17)$$

$$\frac{d\phi}{dt} = \frac{V\cos\gamma\cos\psi}{(r_m+h)} \quad (18)$$

$$\frac{d\theta}{dt} = \frac{V\cos\gamma\sin\psi}{\cos\phi(r_t+h)} \quad (19)$$

$$\frac{dh}{dt} = V\sin\gamma \quad (20)$$

where m is the aircraft mass, V is the aerodynamic speed, T is the thrust magnitude, α is the angle of attack, h is the altitude, L is the lift, D is the drag, g is the nominal acceleration of gravity, γ is the flight path angle (FPA), ϕ is the bank or roll angle, ψ is the heading angle, s_{sfc} is the specific fuel consumption, Φ is the geodetic latitude, θ is the geodetic longitude, r_M is the meridional radius of curvature and r_T is the transverse radius of curvature. Additionally, aerodynamic and propulsion parameters are calculated separately.

Detect-and-Avoid system

Both cooperative and non-cooperative DAA systems are being developed to address RPAS safe integration into the non-segregated airspace [15]. The DAA capability can be defined as the automatic detection of possible conflicts (i.e., collision threats) by the RPAS platform and the implementation of avoidance manoeuvres to prevent the identified collision threats. As part of our research, the possible synergies attainable with the adoption of different detection, tracking and trajectory generation algorithms were studied. The combined DAA architecture is depicted in Figure 5 with an identification of primary (solid line) and auxiliary sensors (dashed line) for cooperative and non-cooperative DAA tasks. An analysis of the available DAA candidate technologies and the associated sensors was presented in [16-20]. An approach to the definition of encounter models and their applications

on the DAA strategies is presented in [21] considering both cooperative and non-cooperative scenarios. The error propagation from different sources and the impacts of host and intruders dynamics on the ultimate DAA solution were investigated [18]. The requirements for developing an effective DAA system can be derived from the current regulations applicable for the human pilot see-and-avoid capability. Criticality analysis is carried out to prioritize (i.e. to determine if a collision risk threshold is exceeded for all the tracked intruders) and to determine the action commands. If an avoidance action is required, the DAA system generates and optimises an avoidance trajectory according to a cost function defined by {minimum distance, fuel, time and closure rate} with the aid of differential geometry algorithms to generate a smooth trajectory.

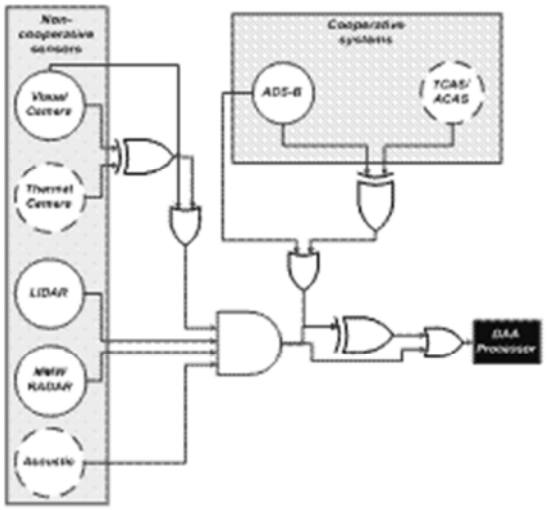

Figure 5 DAA system architecture

In the non-cooperative scenario, the system employs navigation-based image stabilization with image morphology operations and a multi-branch Viterbi filter for obstacle detection, which allows heading estimation. The system utilizes a Track-to-Track (T^3) algorithm for data fusion that allows combining data from different tracks obtained with FLS and/or ADS-B depending on the scenario. Successively, it utilizes an Interacting Multiple Model (IMM) algorithm to estimate the state vector allowing a prediction of the intruder trajectory over a specified time horizon. Both in the cooperative and non-cooperative cases, the risk of collision is evaluated by setting a threshold on the Probability Density Function (PDF) of a Near Mid-Air Collision (NMAC) event over the separation area. So, if the specified threshold is exceeded, an avoidance manoeuvre is performed based on a heading-based Differential Geometry (DG) algorithm and optimized utilizing a cost function with minimum time constraints and fuel penalty criteria weighted as a function of separation distance. A dedicated analysis is performed to determine the overall uncertainty volume in the airspace surrounding the intruder track. This is accomplished by considering both the navigation and tracking errors affecting the measurements and translating them to unified range and bearing uncertainty descriptors. In order to quantify the errors, let σ_{Ex}, σ_{Ey} and σ_{Ez} represent the standard deviations of the navigation error $(\sigma_{nx}, \sigma_{ny}, \sigma_{nz})$ and tracking error $(\sigma_{tx}, \sigma_{ty}, \sigma_{tz})$ in the x, y and z cardinal directions respectively. The range and bearing errors associated with the intruder tracking process are transformed into a local Cartesian coordinate frame (either host or intruder body frame). The overall uncertainty volume is obtained by combining these two error ellipsoids using spherical harmonics decomposition [17].

ABIA/DAA systems integration

The ABIA/DAA integrated architecture is illustrated in Figure 6. The Position, Velocity and Attitude (PVA) measurements are obtained from an Extended Kalman Filter (EKF) that fuses data from GNSS and other navigation sensors [22-27].

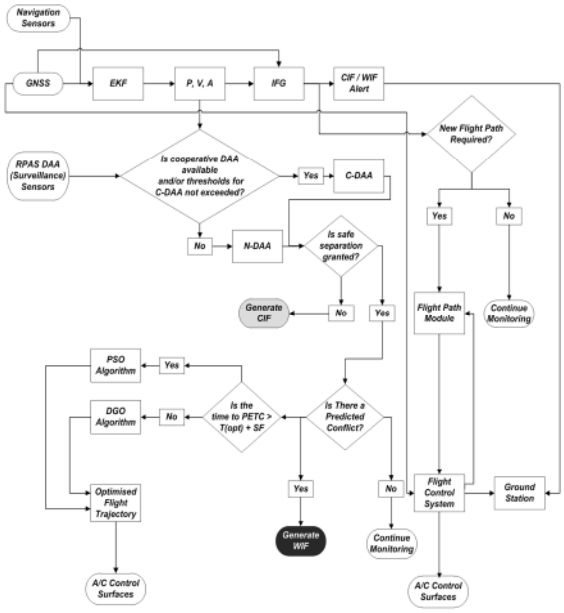

Figure 6 ABIA/DAA integrated architecture

Based on availability, either C-DAA or N-DAA sensors are used for granting safe separation. In parallel, the ABIA flight path optimization process starts when the CIF is generated. Pseudospectral Optimisation (PSO) or Differential Geometry Optimization (DGO) techniques are used to generate a set of optimal trajectory solutions free of near mid-air conflicts and integrity degradations. The selection of PSO or DGO is based on the available time horizons for the ABIA and DAA processes. The Frenet-Serret equations are used to describe host RPAS/intruder relative motion [16] and a minimum

separation distance is defined taking into account the combined navigation/tracking uncertainty volume. If the distance between the RPAS and the moving intruder is or will be less than the separation distance at a specific time interval, then a conflict condition is established. Time and fuel are used as criteria in the cost functional (applying different weightings to obtain a set of feasible solutions), the dynamic model is used as the dynamic constraint, and satellite elevation criteria are used as path constraints. Boundary conditions are set from the values of flight parameters when the CIF is generated. The selection of the optimal trajectory from the generated set of safe trajectories is performed is based on minimisation of the following cost function [19, 20]:

$$J = w_t \cdot t_{SAFE} + w_f \int [SFC \cdot T(t)]dt + \\ -w_d \cdot D_{min} - w_{id} \cdot \int D(t)dt \quad (21)$$

where:

- $D(t)$ is the estimated distance of the generated avoidance trajectory points from the avoidance volume associated with the obstacle.
- $D_{min} = \min[D(t)]$ is the estimated minimum distance of the avoidance trajectory from the avoidance volume.
- $t_{SAFE} = t|_{D_{min}}$ is the time at which the safe avoidance condition is successfully attained.
- SFC $[\frac{kg}{N} \cdot s]$ is the specific fuel consumption.
- $T(t)$ is the thrust profile.
- w_t, w_f, w_d, w_{id} are the weightings attributed to time, fuel, distance and integral distance respectively.

In time-critical avoidance applications (i.e., closing-up obstacles with high relative velocities) appropriate higher weightings are used for the time and distance cost elements.

Simulation case studies

A number of simulation case studies were performed to evaluate the performance of the ABIA and integrated ABIA/DAA systems. A GNSS constellation simulator (GCS) was developed to calculate GNSS satellite position and velocity in the Earth-Centred Earth-Fixed (ECEF) reference frame and to obtain satellite visibility data from any point along the aircraft flight trajectory. The GCS was implemented in MATLAB® to simulate both GPS and GALILEO constellations. The satellite position and velocity were calculated from the Kepler's laws of orbital motion using either the YUMA or SEM almanac data [28, 29] for GPS and a standard Walker constellation (27/3/1), which means 27 satellites in three Medium Earth Orbit (MEO) planes with 1 active spare satellite per orbital plane. The selected ABIA/DAA host platform was the AEROSONDE RPAS and various geometric parameters were extracted from the literature to draw a detailed 3-D model of this aircraft [30].

ABIA IFG Simulation

In order to validate the design of the ABIA IFG module, a MATLAB® simulation activity was performed employing the algorithms developed during this research. The simulated AEROSONDE RPAS trajectory included the following flight phases:

- Climb phase (0-300s);
- Turning climb phase (300-600s);
- Straight and level (cruise) phase (600-900s);
- Level turn phase (900-1200s)
- Turn and descend phase (1200-1500s);
- Approach (straight) phase (1500-1800s);

The combined GPS/GALILEO constellation was simulated and the GNSS receiver tracking loops were modelled with a flat random vibration power curve from 20Hz to 2000Hz with amplitude of $0.005 g^2/Hz$ and the oscillator vibration sensitivity $S_u(f_m) = 1 \times 10^{-9}$ parts/g. All CIFs and WIFs relative to antenna masking, geometric accuracy degradations, SNR, multipath and Doppler shift were generated. The main results obtained with the simulated GPS constellation are shown in Table 1.

Table 1 GPS constellation simulation results

	CIF	WIF
Climb	---	---
Turning Climb	334~374s, 426~446s 517~558s	---
Cruise	874~900s	---
Level Turn	901~1200s	903~906s, 913s, 920~924s, 930~931s, 938~942 s, 948~949s, 956~959s, 966~967s, 974~977s, 984~985s, 992~995s, 1002~1003s, 1110~1113s, 1020~1021s, 1028~1031s, 1128~1129s, 1136~1139s, 1146~1147s, 1154~1157s, 1164~1165s, 1172~1175s, 1182~1183s, 1190~1192s, 1200s
Turning Descent	1201~1441s, 1448~1464s, 1471~1487s 1494~1500s	1204s, 1223~1224s, 1247~1249s, 1272~1273s, 1296~1297s, 1320~1321s, 1344~1367s, 1368s, 1391~1392s, 1414~1415s, 1438~1439s, 1461~1462s, 1484~1485s
Descent	1503~1800s	---

In some cases, the CIF was generated but it was not followed by the WIF (this was due to a temporary adverse relative geometry not leading to GNSS signal losses). During the level turn and turning descent phases, the CIF was followed by the WIF. It was also observed that the CIF was always triggered at least 2 seconds before the successive WIF onset (up to 13 seconds in one case during the turning descent phase). These results are consistent with previous ABIA research on manned aircraft applications [1, 2, 3] and corroborate the validity of the models developed for the CIF/WIF thresholds. It is evident that the availability of a usable CIF represents a significant progress in this research with the potential for both manned aircraft and RPASs to recover from mission- and safety-critical flight conditions potentially leading to GNSS data losses. Therefore, it is envisaged that a properly designed ABIA FPM could take full advantage of this predictive behaviour, allowing the RPAS to correct its flight trajectory/attitude in order to avoid the occurrence of the critical GNSS data losses. Additionally, it is possible that this predictive behaviour be exploited in the pursuit of a GNSS based auto-landing capability. These results corroborate the validity of the models developed for the CIF/WIF thresholds. It was also observed that the CIF was always triggered at least 2 seconds before the successive WIF onset. This evidence is particularly important for the ABIA system design. In fact, it is evident that the availability of a usable CIF represents a significant progress in this research with the potential for both manned aircraft and RPASs to recover from mission- and safety-critical flight conditions potentially leading to GNSS data losses. Therefore, it is envisaged that a properly designed ABIA FPM could take full advantage of this predictive behaviour, allowing the RPAS to correct its flight trajectory/attitude in order to avoid the occurrence of the critical GNSS data losses. Additionally, it is possible that this predictive behaviour be exploited in the pursuit of a GNSS based auto-landing capability.

ABIA/DAA simulation

The integration of ABIA into an existing RPAS DAA architecture was studied in various C-DAA and N-DAA scenarios. The test platforms used were:

- AEROSONDE RPAS (ABIA/DAA host platform);
- AIRBUS 320 (A320) and AEROSONDE RPAS intruders.

In all test cases, an avoidance volume (sum of navigation and tracking errors) was generated by the DAA system [17]. PSO or DGO techniques were used to generate the new (optimal) trajectory based on the available time to conflict (i.e., host entering the avoidance volume). The avoidance trajectory was initiated by the DAA system when the probability of collision exceeded the required threshold value. Time, fuel, distance and integral distance were used in the cost functional, the RPAS 3-DOF dynamic model was used as dynamic constraint, and the minimum elevation criteria as path constraint for both PSO and DGO techniques. Boundary conditions were set from the values of the flight parameters at the first CIF epoch. Figure 7 illustrates the C-DAA test scenario where two AEROSONDE RPASs (1 ABIA host platform and 1 intruder) are 90° off track on the same Flight Level (FL). The risk of collision is detected and resolved. The host RPAS platform equipped with ABIA/DAA is able to generate an avoidance trajectory which is free from CIF/WIF occurrences. As depicted in Figure 7, the host RPAS DAA avoidance trajectory and the ABIA/DAA avoidance trajectory have a different rejoin point on the original track. To provide clarity, three different points are shown on the ABIA/DAA host platform trajectory:

- DAA Break-off Point: Corresponding to the point where the host UA initiates the avoidance trajectory (commanded by the DAA system). The cost function criteria adopted in this case is minimum time.
- DAA Safe Manoeuvring Point: Corresponding to the point where the host RPAS can manoeuvre safely (any manoeuvre within its operational flight envelope) has 0 ROC. From this point onwards the DAA cost function criteria switches to minimum time and minimum fuel to get back on the original (desired) track.
- ABIA Re-join Point: Corresponding to the point where the host RPAS re-joins the original (desired) track without GNSS data degradations.

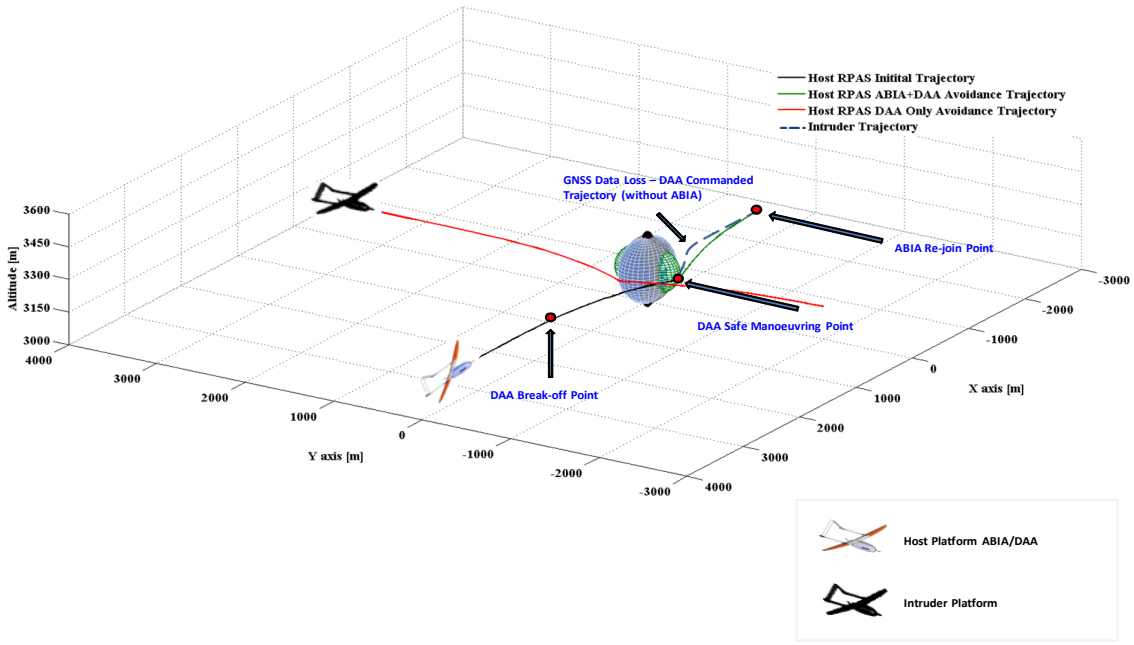

Figure 7 Simulation scenario and illustration of reference points

The horizontal separation and predicted conflict probability in this case are shown in Figure 8 and 9 respectively.

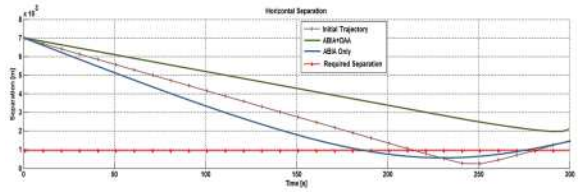

Figure 8 Obtained horizontal separation

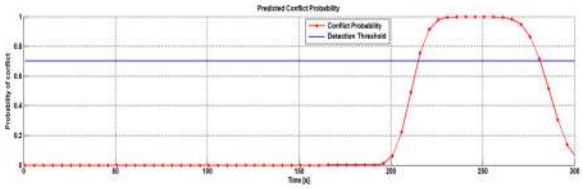

Figure 9 Predicted conflict probability

Figure 10 illustrates the N-DAA test scenario where the AEROSONDE RPAS (ABIA/DAA host platform) and an A320 are flying on the same FL but 90° off track to each other.

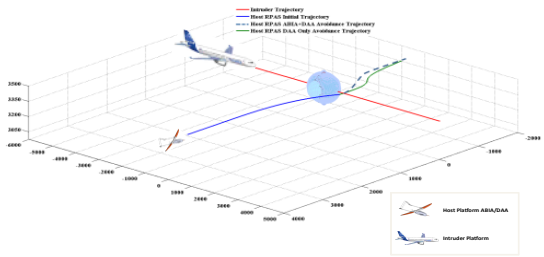

Figure 10 90º non-cooperative DAA scenario

The horizontal and vertical separation obtained is illustrated in Figure 11.

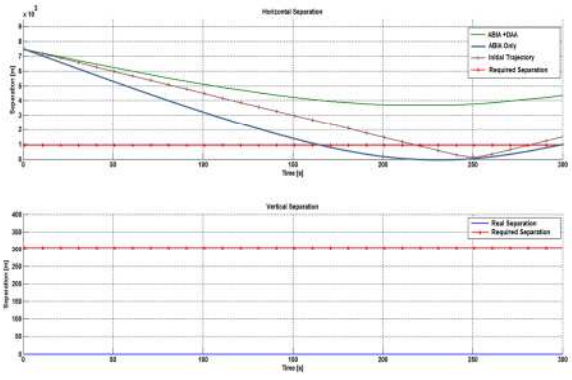

Figure 11 Horizontal and vertical separation

Figure 12 illustrates a C-DAA test scenario where the ABIA host platform (AEROSONDE RPAS) and two intruders (two other AEROSONDE RPASs) are on the same FL.

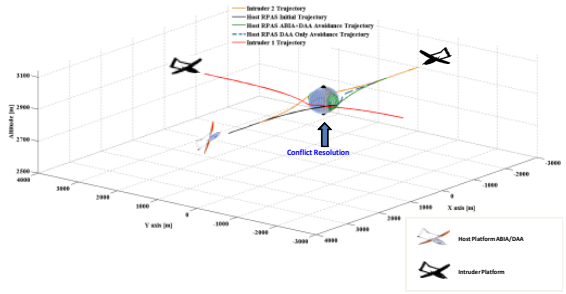

Figure 12 Three RPAS cooperative DAA scenario

One intruder RPAS is 90° off track and the other is following a head-on path with the host RPAS. The horizontal and vertical separation obtained with respect to intruder 1 and 2 are illustrated in Figure 13 and 14 respectively.

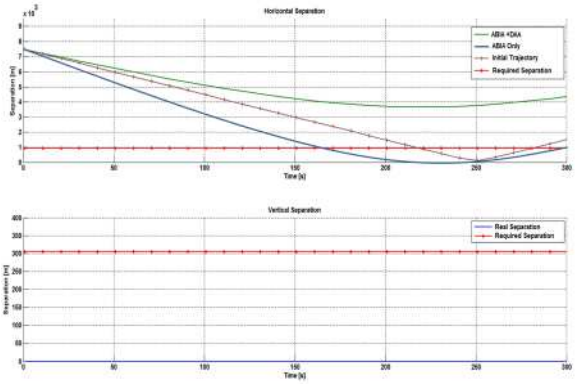

Figure 13 Horizontal and vertical separation of intruder 1

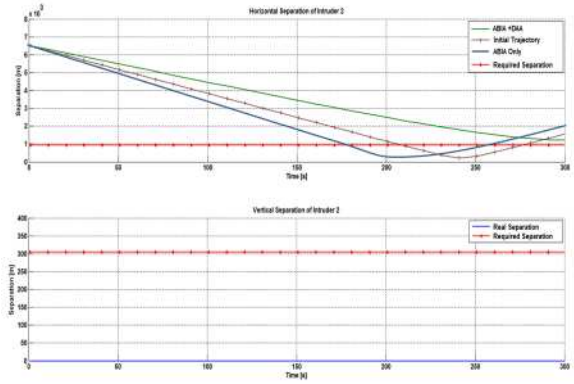

Figure 14 Horizontal and vertical separation of intruder 2

The simulation results demonstrate that the ABIA IFG module is capable of generating integrity flags to provide both caution and warning signals when GNSS signals are degraded or lost. After the integrity caution flag is generated, the time available for the pilot/autopilot to react (before the integrity event is detected and the warning flag is generated), is at least 2 seconds. This TTC can support safety-critical tasks including GLS curved/segmented precision approach and automatic landing applications. Data analysis shows that the ABIA system can provide useful integrity signals for CAT-III precision approach and automatic landing (automated and real-time FPO is essential in this case). In the C-DAA and N-DAA scenarios investigated and in the dynamic conditions explored, all near mid-air collision threats were successfully avoided by implementing adequate trajectory optimisation algorithms. Both PSO and DGO algorithms proved successful in C-DAA and N-DAA scenarios depending on the available time for the optimisation loops (distance host-intruders and relative dynamics).

Conclusions and future work

In this research the synergies between a GNSS ABIA system and a novel RPAS DAA architecture for cooperative and non-cooperative applications were explored. The integration of ABIA with DAA leads to an Integrity Augmented DAA (IAS) solution, which can potentially support the safe and unrestricted access of RPAS to commercial airspace. Simulation case studies were performed for the ABIA IFG module, IFG/FPOM modules and ABIA/DAA integration. The trajectory optimization problem was mathematically formulated and the real-time capability of the FPOM was verified. From the results of the simulation activity, the following conclusions are drawn:

- The ABIA IFG module is capable of generating integrity flags to provide both caution (predictive) and warning signals to the pilot when GNSS signals are degraded or lost.
- After the CIF is generated, the time available for the pilot/autopilot to react before the WIF is generated, is sufficient for safety-critical tasks including GLS curved/segmented approach and automatic landing applications.
- Data analysis shows that the ABIA system can provide the level of integrity required for CAT-IIIC precision approach, which are currently unavailable with LAAS.
- The ABIA integration into an existing RPAS DAA architecture proved that all near mid-air collision threats were successfully avoided by implementing suitable trajectory optimisation

algorithms.

- The proposed ABIA/DAA integration architecture is capable of achieving adequate performance by avoiding critical satellite data losses while fulfilling the separation requirements set for DAA.

Additional long-term objectives of this research include the following:

- Investigate and compare different types of avionics sensor technologies and their potential to support the design of robust ABAS/ABIA architectures for manned aircraft and RPASs.
- Extend the ABAS/ABIA concepts to the Aeronautical Data Link (ADL) application domain and investigate ABIA Line-of-Sight (LOS) and Beyond-Line-of-Sight (BLOS) communication interfaces for RPAS applications.
- Investigate ABIA evolutions for Next Generation Flight Management System (NG-FMS) applications [31-36]:
  - Trajectory Optimization for Future CNS+A systems.
  - 4DT Intent Based Operations.
  - NG-FMS/ABIA Integration.
- Study possible applications of the ABAS/ABIA concepts to advanced mission planning and forensic (accident investigation) applications.
- Evaluate the potential of ABAS/ABIA to enhance the performance of next generation CNS/ATM systems for Performance/Intent Based Operations (PBO/IBO) and Four-Dimensional Trajectory (4DT) management [37].

References

1. Sabatini R, Moore T, Hill C, A New Avionics Based GNSS Integrity Augmentation System: Part 1 – Fundamentals, *Journal of Navigation*, vol. 66, no. 3, pp. 363-383, May 2013. DOI: 10.1017/S0373463313000027
2. Sabatini R, Moore T, Hill C, A New Avionics Based GNSS Integrity Augmentation System: Part 2 – Integrity Flags, *Journal of Navigation*, vol. 66, no. 4, pp. 511-522, June 2013. DOI: 10.1017/S0373463313000143
3. Sabatini R, Moore T, Hill C, A Novel GNSS Integrity Augmentation System for Civil and Military Aircraft, *International Journal of Mechanical, Aerospace, Industrial and Mechatronics Engineering*, vol. 7, no. 12, pp. 1433-1449, International Science Index, December 2013.
4. Sabatini R, Moore T, Hill C, A Novel Avionics-Based GNSS Integrity Augmentation System for RPAS Applications, *Paper presented at the Royal Institute of Navigation (RIN) Conference on Unmanned Air Vehicles - Sharing the Airspace*, Teddington (UK), February 2013.
5. Sabatini R, Moore T, Hill C, Avionics Based GNSS Integrity Augmentation for Mission- and Safety-Critical Applications, *Paper presented at 25th International Technical Meeting of the Satellite Division of the Institute of Navigation: ION GNSS-2012*, Nashville (Tennessee), September 2012.
6. Kaplan ED, Hegarty CJ, *Understanding GPS: Principles and Applications*, Artech House, Second Edition, 2006.
7. RTCA DO-245A, Minimum Aviation System Performance Standards for Local Area Augmentation System (LAAS), Dec 2004.
8. Mubarak OM, Dempster AG, Analysis of Early Late Phase in Single and Dual Frequency GPS Receivers for Multipath Detection, The University of New South Wales (Australia), 2010. Available at http://www.gmat.unsw.edu.au/snap/staff/omer_mubarak.htm.
9. Ward P, Using a GPS Receiver Monte Carlo Simulator to Predict RF Interference Performance, *Proceedings of 10th International Technical Meeting of The Satellite Division of The Institute of Navigation*, pp.1473–1482, Kansas City, MO, USA, September 1997.
10. Ward P, GPS Receiver RF Interference Monitoring, Mitigation, and Analysis Techniques, *Navigation - Journal of the Institute of Navigation*, vol. 41, no. 4 (Winter), pp. 367-391, 1994-95.
11. Sabatini R, Palmerini G, Differential Global Positioning System (DGPS) for Flight Testing, NATO Research and Technology Organization (RTO) – Systems Concepts and Integration Panel (SCI), AGARDograph Series RTO-AG-160, vol. 21, Oct 2008.
12. Braasch MS, On the Characterization of Multipath Errors in Satellite-based Precision Approach and Landing Systems, College of Engineering and Technology, Ohio University, June 1992.
13. Conley R, Wilfong A, The Design and Application of a GPS Integrity Model, Fourth International Technical Meeting of the Satellite Division of The Institute of Navigation, ION GPS, pp. 739-752, September 1991.
14. Leasure SL, Parrott D, Thomas J, High-Dynamic Stand-Alone GPS Navigation - the Limits of a Reversionary Mode, Fourth International Technical Meeting of the Satellite Division of The Institute of Navigation, ION GPS, pp. 453-458, September 1991.
15. Hottman SB, Hansen KR, Berry M, Literature Review on Detect, Sense, and Avoid Technology for Unmanned Aircraft Systems, Tech. Report DOT/FAA/AR-08/41, US Department of Transport, USA, 2009.
16. Muraru A, A Critical Analysis of Sense and Avoid Technologies for Modern UAVs, *Advances in Mechanical Engineering*, ISSN: 2160-0619, vol. 2, no.1, March 2012. DOI:10.5729/ame.vol2.issue1.23
17. Ramasamy S, Sabatini R, Gardi A, Avionics Sensor Fusion for Small Size Unmanned Aircraft Sense-and-Avoid, *Paper presented at IEEE Workshop on Metrology for Aerospace*, pp. 271-276, Benevento, Italy, May 2014. DOI: 10.1109/MetroAeroSpace.2014.6865933.

18. Rodriguez P, Sabatini R, Gardi A, Ramasamy S, A Novel System for Non-Cooperative RPAS Sense-and-Avoid, *Paper presented at European Navigation Conference 2013*, Vienna, Austria, April 2013.
19. Sabatini R, Gardi A, Ramasamy S, A Laser Obstacle Detection and Avoidance System for Unmanned Aircraft Sense-and-Avoid, *Applied Mechanics and Materials*, Vol. 629, Trans Tech Publications, Switzerland, pp. 355-360, 2014. DOI: 10.4028/www.scienti fic.net/AMM.629.355.
20. Sabatini R, Gardi A, Richardson MA, LIDAR Obstacle Warning and Avoidance System for Unmanned Aircraft, *International Journal of Mechanical, Aerospace, Industrial and Mechatronics Engineering*, vol. 8, no. 4, pp. 62-73, International Science Index, April 2014.
21. Kochenderfer MJ, Espindle LP, Griffith JD, Kuchar JK, Encounter Modeling for Sense and Avoid Development, *Paper presented at Integrated Communications, Navigation and Surveillance Conference (ICNS)*, pp. 1-10, 2008. DOI: 10.1109/ICNSURV.2008.4559177.
22. Sabatini R, Ramasamy S, Gardi A, Salazar LR, Low-cost Sensors Data Fusion for Small Size Unmanned Aerial Vehicles Navigation and Guidance, *International Journal of Unmanned Systems Engineering*, vol. 1, no. 3, pp. 16-47, August 2013.
23. Sabatini R, Richardson MA, Airborne Laser Systems Testing and Analysis, NATO Research and Technology Organization (RTO) – Systems Concepts and Integration Panel (SCI), AGARDograph Series RTO-AG-300, vol. 26. 2010.
24. Sabatini R, Bartel C, Kaharkar A, Shaid T, Ramasamy S, Navigation and Guidance System Architectures for Small Unmanned Aircraft Applications, *International Journal of Mechanical, Aerospace, Industrial and Mechatronics Engineering*, vol. 8, no. 4, pp. 733-752, International Science Index, April 2014.
25. Sabatini R, Cappello F, Ramasamy S, Gardi A, Clothier R, An Innovative Navigation and Guidance System for Small Unmanned Aircraft using Low-Cost Sensors, In press, *Aircraft Engineering and Aerospace Technology*, Emerald Publishing Group Ltd., 2015 (In press).
26. Sabatini R, Rodriguez L, Kaharkar A, Bartel C, Shaid T, Carrier-Phase GNSS Attitude Determination and Control System for Unmanned Aerial Vehicle Applications, ARPN Journal of Systems And Software, vol. 2, 2012.
27. Sabatini R, Rodríguez L, Kaharkar A, Bartel C, Shaid T, Zammit-Mangion D, Low-Cost Navigation and Guidance Systems for Unmanned Aerial Vehicles—Part 2: Attitude Determination and Control, Annual of Navigation, vol. 20, pp. 97-126, 2013.
28. YUMA GPS Almanacs. Available at: http://www.celestrak.com/GPS/almanac/Yuma/definition.asp.
29. SEM GPS Almanacs. Available at: http://www.celestrak.com/GPS/almanac/SEM/definition.asp.
30. Burston MT, Sabatini R, Clothier R, Gardi A, Ramasamy S, Reverse Engineering of a Fixed Wing Unmanned Aircraft 6-DoF Model for Navigation and Guidance Applications, Applied Mechanics and Materials, vol. 629, Trans Tech Publications, Switzerland, pp. 164-169, 2014. DOI: 10.4028/www.scientific.net/AMM.629.164.
31. Sabatini R, Liu Y, De Ridder K, Gardi A, Ramasamy S, Zammit-Mangion D, Rodriguez L, ENDEAVOUR Project – Novel Avionics and ATM Systems for SESAR and NextGen, *Paper presented at the Conference Avionics Europe 2013 – Tackling the Challenges in Avionics: Single Sky Many Platforms*, Munich, Germany, February 2013.
32. Ramasamy S, Sabatini R, Gardi A, Kistan T, Next Generation Flight Management System for Real-Time Trajectory Based Operations, *Applied Mechanics and Materials*, Vol. 629, Trans Tech Publications. Switzerland, pp. 344-349, 2014. DOI:10.4028/www.scientific.net/AMM.629.344.
33. Ramasamy S, Sangam M, Sabatini R, Gardi A, Flight Management System for Unmanned Reusable Space Vehicle Atmospheric and Re-entry Trajectory Optimisation, *Applied Mechanics and Materials*, vol. 629, Trans Tech Publications, Switzerland, pp. 304-309, 2014. DOI: 10.4028/www.scientific.net/AMM.629.304.
34. Gardi A, Sabatini R, Ramasamy S, Kistan T, Real-Time Trajectory Optimisation Models for Next Generation Air Traffic Management Systems, *Applied Mechanics and Materials*, Vol. 629, Trans Tech Publications. Switzerland, pp. 327-332, 2014. DOI: 10.4028/www.scientific.net/AMM.629.327.
35. Gardi A, Sabatini R, Ramasamy S, de Ridder K, 4-Dimensional Trajectory Negotiation and Validation System for the Next Generation Air Traffic Management, AIAA Guidance, Navigation & Control Conference 2013 (GNC 2013), Boston, Massachusetts (USA), August 2013. DOI: 10.2514/6.2013-4893.
36. Ramasamy S, Sabatini R, Gardi A, Liu Y, Novel Flight Management System for Real-Time 4-Dimensional Trajectory Based Operations, AIAA Guidance, Navigation & Control Conference 2013 (GNC 2013), Boston, Massachusetts (USA), August 2013. DOI: 10.2514/6.2013-4763.
37. Sabatini R, Moore T, Hill C, Avionics-Based GNSS Integrity Augmentation for Unmanned Aerial Systems Sense-and-Avoid, *Paper presented at 26th International Technical Meeting of the Satellite Division of the Institute of Navigation: ION GNSS+ 2014*, Tampa (Florida, USA), 2014.